Impact of the metal centre (Al 3+ , Fe 3+) on the post-synthetic lithiation of functionalized MIL-53s and the electrochemical properties of lithiated derivatives

Morgane Denis, Hubert Chevreau, Pablo Salcedo-Abraira, Philippe Moreau, Nicolas Dupré, Michael Paris, Philippe Poizot, Thomas Devic

Impact of the metal centre (Al^{3+}, Fe^{3+}) on the post-synthetic lithiation of functionalized MIL-53s and electrochemical properties of the lithiated derivatives

Morgane Denis,[a] Hubert Chevreau,[b] Pablo Salcedo-Abraira,[a] Philippe Moreau,[a] Nicolas Dupré,[a] Michael Paris,[a] Philippe Poizot[a] and Thomas Devic*[a]

Abstract

Metal-Organic Frameworks (MOFs) combining both organic and inorganic redox-active moieties have recently found their interest in the field of the electrochemical energy storage. We here focused our attention on MIL-53(M) (M = Al, Fe) analogues based on 2,5-dioxo-1,4-benzenedicarboxylate, as this ligand was already found to present an interesting electrochemical activity based on the quinone/phenolate redox couple in the solid state. We described here our attempts to chemically lithiate the title solids. Various synthetic paths were explored, and the resulting solids were characterized by a broad set of techniques, including X-ray diffraction, solid state NMR, transmission electron microscopy, inductively coupled plasma - atomic emission spectroscopy analysis and total X-ray scattering experiments, among others. We showed that although the lithiation is accompanied by a loss of the long-range order whatever the synthetic conditions and the trivalent cation, the reactivity strongly differs for M = Al and Fe. Eventually, the electrochemical extraction/uptake of Li^+ in the lithiated derivatives was evaluated in Li-half cells. Although the storage capacities are moderate, we found that the presence of even a minor amount of M^{3+} cation not only impacts on the working potential of the ligand, but also improves the long term capacity retention.

Introduction

Apart from the traditional applications related to sorption (storage, capture, separation, controlled release, sensing,…), Metal Organic Frameworks (MOFs) have been proposed as potential electrode materials for the electrochemical energy storage.[1–7] Although unable (yet ?) to compete with conventional inorganic and organic electrode materials, MOFs offer interesting features, such as (i) the possibility to combine multiple redox centres (this is nevertheless sometimes achievable in inorganics through anionic redox), and (ii) their microporosity, which might favour ionic transport. When used as negative electrode materials, their reduction at low potential is accompanied by an irreversible conversion into polyphasic systems. On the opposite, when used as a positive electrode materials,[4] few solids can be reversibly oxidized/reduced through a conventional insertion mechanism. MIL-53(Fe) (MIL stands for Materials Institute Lavoisier), with the chemical formula $Fe^{III}(OH)(BDC)$ (BDC = 1,4-benzenedicarboxylate), was the first MOF studied for this purpose. This solid delivers ~70 mAh g^{-1} at ~3.0 V *vs.* Li^+/Li, this activity being related to the reversible reduction of ca. half of Fe^{III} to Fe^{II}.[8] 2,5-dioxo-1,4-benzenedicarboxylate (known as DOBDC and *p*-DHT in the fields of MOFs and electrochemical energy storage, respectively) is a terephthalate derivative known to be redox active, not only in solution,[9] but also in the solid state,[10,11] this activity being associated with the quinone/phenolate redox couple. Noteworthy, some of use showed that, when employed as a positive electrode in an electrochemical half-cell, the redox potential could be tuned by playing with the surrounding cations, increasing from 2.55 to almost 3.5 V *vs.* Li^+/Li when moving from $Li_4(DOBDC)$ to $MgLi_2(DOBDC)$, while maintaining a decent capacity (close to 100 mAh g^{-1}).[12]

With this in mind, we were interested in combining the redox activity of this organic ligand with that of a transition metal (TM) cation. MOFs containing both DOBDC and TM are known, and can be divided in two subclasses: (i) those containing fully deprotonated linkers (charge -4) bound to TM through both the carboxylate and phenolate moieties,[13–18] the most famous member being CPO-27/MOF-74, with the chemical formula M^{II}_2(DOBDC), and (ii) those containing ligands with proton remaining on the phenolic oxygen (charge -2) and the TM interacting solely with the carboxylate groups,[19–22] such as functionalized analogues of MIL-53(Fe), MIL-88(Fe) and UiO-66(Zr). The first ones are *a priori* not suitable materials for electrochemical energy storage, as the redox activity would require the displacement of polyvalent cations (except if the initial solid also contain charge compensating monocations, or if the redox-activity is accompanied by anion rather than cation insertion[23]). For the second series, the access to the quinone/phenolate redox couple in standard battery electrolytes (anhydrous, aprotic) first requires the chemical lithiation (*e.g.* through an acid-base reaction) of the phenolic groups. This approach was very recently successfully applied by the Vlad group to a Mn-DOBDC MOF, leading to a mixed electrochemical activity around 3.2 V *vs.* Li^+/Li, but with a modest reversible capacity (~60 mAh g^{-1}).[24] Considering the already reported electrochemical activity of MIL-53(Fe), we focused our attention on its relative based on DOBDC, namely MIL-53(Fe)-$(OH)_2$ or Fe(OH)(H_2DOBDC) (Figure 1).[20] For the sake of comparison, the analogue built up from redox inert Al^{3+}, MIL-53(Al)-$(OH)_2$,[25] was also considered.

We will here describe our attempts to produce *fully lithiated* DOBDC-based MIL-53s (Li_3MO(DOBDC) , M = Al, Fe) by post-synthetic basic treatments. Through a broad set of characterization tools, including powder XR diffraction (PXRD), infrared (IR) spectroscopy, ^{13}C and ^{27}Al solid state nuclear magnetic resonance (NMR), thermogravimatric analyses (TGA), inductively coupled plasma-atomic emission spectroscopy (ICP-AES) analysis, scanning transmission electron microscopy-energy *dispersive* X-ray analysis (STEM-EDX) and total X-ray scattering experiments, we will show that although the lithiation is accompanied by the collapse of the structure whatever the trivalent cation, the composition of the final product of lithiation strongly differs for Al and Fe. Eventually, the electrochemical properties of the lithiated MOFs will also be presented and compared to the ones of the fully lithiated ligand Li_4(DOBDC).

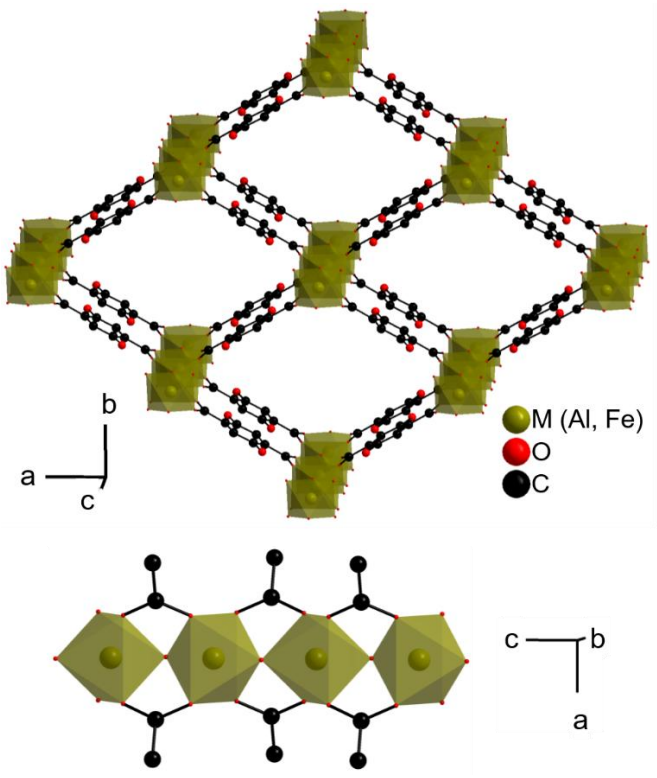

Figure 1. Crystal structure of MIL-53(M)-$(OH)_2$ or M(OH)(H_2DOBDC).[20] Top: view along the pores axis, bottom: view of the inorganic chain. Protons (bound to C, organic O and inorganic O) are omitted, and only one out of the two disordered positions of the phenolic groups is shown.

Experimental

Synthetic procedures

Syntheses of pristine MOFs were carried out in air, while lithiation experiments were conducted in a glove box filled with Ar.

MIL-53(Al)-$(OH)_2$ was prepared in *N*,*N*-diethylformamide (DEF) according to the published procedure.[25] The solvent was removed from the pores in two steps (DEF-water exchange followed by a thermal activation). First, the as-synthesized solid was dispersed in a 1:1 mixture of water and methanol, heated at 150°C in an autoclave for 12 hours, and recovered by filtration. This solid was further dried at 180°C under vacuum for 16 hours, affording the activated form of MIL-53(Al)-$(OH)_2$, as evidenced by PXRD (see Figures S1-S4 and Table S1 for details).

MIL-53(Fe)-$(OH)_2$ was also prepared from the reported procedure, that time in *N*,*N*-dimethylformamide (DMF).[20] The last step (washing with ethanol and drying in air) was sufficient to obtain the hydrated compound. This solid was dried at 150°C under vacuum for 16 hours, to lead to the partially activated form of MIL-53(Fe)-$(OH)_2$.

Lithiation of MIL-53(Al)-$(OH)_2$ with LiH in DMF

50.0 mg (0.21 mmol, 1 eq.) of dry MIL-53(Al)-$(OH)_2$ or Al(OH)(H_2DOBDC) and 5.1 mg (0.64 mmol, 3 eq.) of LiH were placed together with 5 mL of anhydrous DMF in a schlenk filled with Ar. The mixture was heated at 130°C under stirring for 16 hours. The colour of the suspension evolved from pale yellow to orange. The resulting solid was recovered by filtration, washed with anhydrous tetrahydrofurane (THF), and dried at 150°C under vacuum for 16 hours.

Lithiation of MIL-53(Al)-$(OH)_2$ with LiOMe in MeOH/THF

50.0 mg (0.21 mmol, 1 eq.) of dry MIL-53(Al)-$(OH)_2$ or Al(OH)(H_2DOBDC) were placed in 4 mL of a 1:1 mixture anhydrous of tetrahydrofuran (THF) and methanol (MeOH) in a schlenk filled with Ar. 0.284 mL (0.63 mmol, 3 eq.) of a 2.2 M solution of LiOMe in MeOH were added. The mixture was heated at 50°C under stirring for 16 hours. No drastic colour change was observed. The resulting solid was recovered by filtration, washed with anhydrous MeOH and THF, and dried at 180°C under vacuum for 16 hours.

Lithiation of MIL-53(Fe)-$(OH)_2$ with LiOMe in MeOH/THF

50.0 mg (0.19 mmol, 1 eq.) of partially dry MIL-53(Fe)-$(OH)_2$ were placed in 4 mL of a 1:1 mixture anhydrous of THF and methanol (MeOH) in a schlenk filled with Ar. 0.254 mL (0.56 mmol, 3 eq.) of a 2.2 M solution of LiOMe in MeOH were added. The mixture was heated at 50°C under stirring for 16 hours. The resulting solid was recovered by filtration, washed with anhydrous MeOH and THF, and dried at 170°C under vacuum for 16 hours.

Materials and methods

Characterization of the pristine MOFs were carried out in ambient conditions, whereas dried and lithiated solids were analysed under inert atmosphere or in sealed sample holders.

Infrared spectra were collected on a FTIR Bruker Vertex 70 spectrometer in transmission mode between 400 and 4000 cm^{-1} on solids diluted in KBr pellets. PXRD patterns were collected either in a Bragg-Brentano mode with a Bruker D8 Advance diffractometer, or in a Debye-Scherrer mode with an INEL XRG3500 diffractometer, both equipped with a Cu anode (λ = 1.5406 Å). Lebail refinements were carried out with the Fullprof suite.[26] TGA were collected under Ar at 5°C min^{-1} up to 800°C on either a Setaram SENSYSevo or a NETZSCH STA 449F3 Jupiter apparatus. For the ICP-AES experiments, solids were first dissolved in a 0.02 or

0.2 M aqueous solution of NaOH (Fe- and Al-based solids, respectively), and further analysed thanks to an iCAP 6300 radial analyser (Thermo Scientific). Scanning electron microscopy (SEM) was carried out on a JEOL JSM-7600F microscope. Samples were pasted on carbon tape and further coated with platinum to improve the surface electronic conductivity. STEM experiments were carried out using a Themis Z G3 Cs-probe corrected microscope from Thermo Fisher Scientific, operating at 80 kV, and equipped with a high-angle annular dark field (HAADF) detector and a superX EDX detector. The solid was deposited onto a lacey carbon film supported by a copper grid. A vacuum transfer sample holder (GATAN 648) was used to prevent any air from contacting the reactive sample before its introduction into the microscope. The ^{1}H-^{13}C cross-polarization and magic angle spinning (CP-MAS) and ^{27}Al MAS NMR spectra were recorded on a 500 MHz Bruker Avance III spectrometer (B_0 = 11.7 T) using a 2.5 mm probehead. For the ^{27}Al spectra, the MAS rate, $\pi/12$ pulse length and recycle delays were set to 25 kHz, 3 µs and 1 s, respectively. For the ^{1}H-^{13}C spectra, the MAS rate and contact time were set to 11 kHz and 8 ms, respectively. ^{27}Al and ^{13}C chemicals shifts were referenced to a 1 M $Al(NO_3)_3$ aqueous solution and to tetramethylsilane (TMS), respectively. All spectra were analysed using the DMfit software.[27] X-ray total scattering experiments were carried out on the beamline CRISTAL at synchrotron Soleil (L'Orme les Merisiers, France) at λ = 0.97015 Å, in a Debye Scherrer configuration. The contribution of the glass sample holder (capillary) was subtracted, and the data were treated with the software PDFgetX3.[28] Solid-state electrochemical experiments were carried out by using a two-electrode Swagelok®-type cell with a Li metal disc as the negative electrode and a glassfiber separator soaked with either a 1 M $LiClO_4$ in propylene carbonate (PC) or 1 M $LiPF_6$ in 1:1 ethylene carbonate (EC) dimethylcarbonate (DMC) electrolyte. The composite positive electrodes were prepared in an argon filled glovebox by grinding the solid and Ketjenblack® EC-600JD (Akzo Nobel) carbon conducting additive to insure proper electronic conduction (MOF:carbon ratio = 66:33 wt%, ca. 3 mg of active material per electrode). The electrochemical cells were then cycled in galvanostatic mode at a rate 1 e^-/1 Li^+ exchanged per ligand in 15 hours within various potential windows starting in oxidation (charging step) by using a MPG-2 multi-channel system (Bio-Logic SAS, Seyssinet-Pariset, France).

RESULTS AND DISCUSSION

Two post-synthetic strategies were proposed in the literature to chemically insert Li^+ into neutral MOFs. The first one relies on a redox reaction: a strongly reducing Li salt is added to the MOF, and the reduction of the ligand or the cation is associated with the insertion of Li^+.[29–32] The second one, which is of interest for us, is based on an acid-base reaction:[33–36] a strong lithium base is added to the MOF, leading to the exchange of protons (organic or inorganic) by Li^+. These approaches have been mainly devoted to the optimisation of the gas sorption properties (e.g., H_2 storage[29] or CO_2 capture[37]) and, except in few rare cases,[32] only a minor amount of Li^+ could be incorporated (typically < 15 at. %) without any significant loss of porosity or crystallinity. We thus here face four challenges:

(i) the quantitative exchange of protons by Li^+. As shown by Himsl et al. on MIL-53-(Al)-OH,[34] the lithiation occurs unselectively on organic and inorganic protons. Three Li^+ per M^{3+} must then be inserted to insure that all phenolic groups are lithiated.

(ii) the base must be small enough to diffuse in the pores, strong enough to deprotonate, but not too nucleophilic to limit the degradation of MOF.[33,34] This could be an even stronger issue when quantitative exchange is targeted.

(iii) MIL-53 derivatives are flexible (the pores size and shape evolve with their content or with external stimuli).[38] For example, when suspended in a liquid, MIL-53(Fe)-$(OH)_2$ could present a close pore form (CP, no porosity), a narrow pore (NP) form (slight adsorption) or a large pore form (LP, high sorption capacity) depending on the nature and the physicochemical characteristics of the solvent.[20] The solvent used for the acid base-reaction must then

obviously solubilize the base at least to some extent, but must also insure the opening of the pores.

(iv) MIL-53(Fe)-$(OH)_2$ is highly hydrophilic, but also less thermally stable than other functionalized MIL-53s (decomposition starts below 200°C, even under vacuum).[20] Dehydration must thus be carried out with care, knowing that residual water in the presence of base might lead to the complete degradation of the material.[39]

With this in mind, two pairs of base and solvent were selected: LiH in DMF,[40] and LiOMe in a mixture of THF and MeOH.[10,24] First experiments were carried out on MIL-53(Al)-$(OH)_2$, which is easier to obtain as a fully dehydrated solid, and could be studied by both ^{13}C and ^{27}Al solid state NMR. In the dehydrated state, the PXRD pattern and unit-cell parameters are indeed consistent with a CP form (Figures 2a, S4 and Table S1, respectively). On the IR spectrum (Figure 2b, orange curve), signals associated with X-H (X = C, O) bonds are also well resolved, with inorganic μ_2-OH, phenolic O-H and aromatic C-H vibration bands clearly distinguishable at 3690, 3352, and 3082 cm^{-1}, respectively. Vibration bands characteristics of the ligand, notably COO_{asym}, aromatic CC and COO_{sym} were also clearly identified at 1585, 1494 and 1471 cm^{-1}, respectively. No residual DEF arising from the solvothermal synthesis is detected (C=O and C-H vibration bands at ~1660 and ~2900 cm^{-1}, respectively). This solid was treated with 3 equivalents of LiH in DMF, which is known to lead to a large pore form.[25] The reaction was performed at high temperature (130°C) to improve the otherwise low solubility of LiH in this solvent. Initially yellow, the suspension turned orange within few hours (Figure S8), suggesting a change of the protonation state of the ligand and/or of its coordination mode.

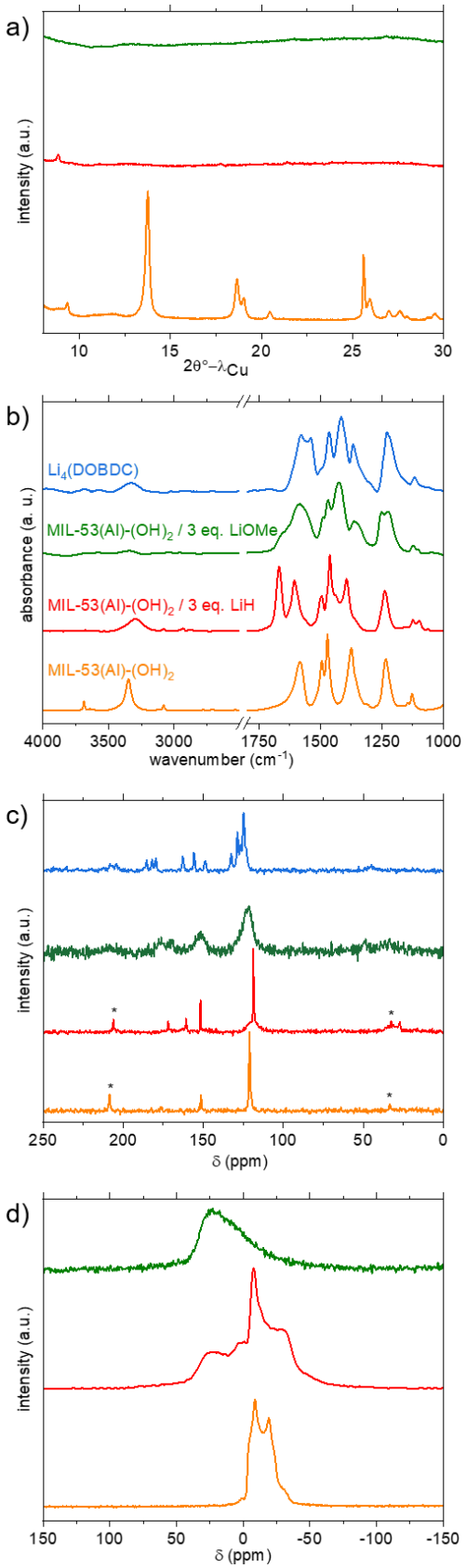

Figure 2. Characterisation of MIL-53(Al)-$(OH)_2$ and its lithiated products. a) PXRD patterns (λ = 1.5406 Å); b) IR spectra; c) ^{1}H-^{13}C CP-MAS NMR spectra (* = spinning side bands); d) ^{27}Al MAS NMR spectra. Data related to dry MIL-53(Al)-$(OH)_2$, Li_4(DOBDC), and lithiation products from LiH-DMF and LiOMe-MeOH/THF, are shown in orange, blue, red and green, respectively.

The final product was thoroughly washed with THF and dried at 150°C under vacuum prior to characterization. Note that attempts to replace THF by MeOH lead to the recovery of the initial colour, suggesting that this change of coordination/protonation state is reversible. The orange product was first studied by PXRD; an almost complete loss of long-range order is observed (Figure 2a, red curve). IR spectroscopy showed the complete disappearance of the signal belonging to inorganic μ_2-OH, while the one characteristics of organic OH groups remained, although with a lower intensity (Figure 2b, red curve). Vibration bands characteristics of the ligand, notably COO_{asym} (1602 cm^{-1}), COO_{sym} (1462 cm^{-1}), and aromatic CC (1494 cm^{-1}) were slightly shifted compared to the pristine solid, in accordance with a modification of the local environment of the ligand. The presence of residual DMF (C=O and C-H vibration bands at 1666 and 2870-3940 cm^{-1}) was also detected. Attempts to remove this solvent by extended washing with THF or dichloromethane, or drying at higher temperature failed, suggesting that DMF is possibly bound, or at least strongly interacting, with the framework. This is in agreement with the thermogravimetric analysis performed under Ar, which does not exhibit a clear plateau corresponding to the desolvated solid prior to the thermal degradation (Figure S10). The relative amount of Li and Al was evaluated by ICP after dissolving the solid in a basic aqueous medium. A ratio Li/Al equal to 1.5 was obtained (expected value = 3), suggesting that only half of the protons were removed, in agreement with the IR analysis. On the solid-state ^{13}C CP-MAS spectrum (Figure 2c, red curve), residual DMF is detected (CH_3 and CO at 27 and 161 ppm, respectively), again in line with the IR study. The signals characteristics of the ligand (COO, CO and Cq+CH at 172, 152 and 119 ppm, respectively) remained visible, although slightly broader and shifted compared to pristine MIL-53(Al)-$(OH)_2$, in agreement with a change of the local surrounding of the ligand upon lithiation. This was confirmed by solid state ^{27}Al NMR spectroscopy. The signal of the dried solid is characteristic of Al^{3+} in a single octahedral site.[41] After lithiation, the spectrum exhibits at least two components, one similar to the pristine material although broadened, and the other one at higher chemical shift and very broad, characteristics of disordered environments (Figure 2d, red curve). To summarize, these synthetic conditions (LiH in DMF) lead only to a partial deprotonation, with a final composition close to $Li_{1.5}AlO(H_{2.5}DOBDC)(DMF)_x$. Attempts to increase the amount of LiH in the reaction medium (up 7 eq.) lead to similar IR spectra (Figure S12) suggesting that this procedure is not suitable to achieve a complete lithiation of MIL-53(Al)-$(OH)_2$.

For this reason, we switched to the second procedure (LiOMe in THF/MeOH), which was recently shown to be successful for the lithiation of a Mn-DOBDC MOF.[24] First experiments were again carried out with MIL-53(Al)-$(OH)_2$, which adopts a large pore conformation when suspended in THF (see Figure S5 and Table S1). This solid was treated with 3 equivalents of LiOMe in a 1:1 mixture of THF and MeOH at 50°C. The solid was ultimately recovered by filtration, washed and dried at 180°C. Contrary to the previous case, no significant colour change was detected. Nevertheless, when exposed to air, the colour very rapidly turned from yellow to green (Figure S9). A similar behaviour was already observed for the parent Li_4(DOBDC°, and was attributed to its oxidation by O_2.[10] This suggests that the lithiation was successful, but that the oxidation potential of the final product is below the one of the redox couple O_2/Li_2O_2 (~3.0 V *vs.* Li^+/Li).

Again, PXRD analysis indicated a full loss of the long-range order upon lithiation (Figure 2a, green curve). On the IR spectrum, no signal belonging to both inorganic and organic OH was detected (Figure 2b, green curve), suggesting that a complete lithiation occurred. This disappearance is accompanied by a shift of the bands characteristic of the core of the ligand (< 1600 cm^{-1}). Although not strictly identical, the spectrum showed some similarities with the one of Li_4(DOBDC) in this region, suggesting that both products are structurally related (Figure 2b). No residual solvent (MeOH, THF) was detected that time, in line with the TG analysis, which showed that the solvent is removed below 130°C, before the thermal degradation of the solid above 250°C (Figure S10). The ICP analysis of the product dissolved in a basic

aqueous medium indicates a ratio Li/Al close to 6-7 (Figure S17), suggesting that a leaching of Al^{3+} occurred during the lithiation. This was confirmed by the analysis of the supernatant of the reaction, which was found to contain a significant amount of aluminium. On the ^{27}Al NMR spectrum, only a broad signal, characteristics of very disordered local environments is visible (Figure 2d, green curve). The ^{1}H-^{13}C CP-MAS NMR spectrum also shows broad signals, but with chemical shifts similar to those of Li_4(DOBDC).

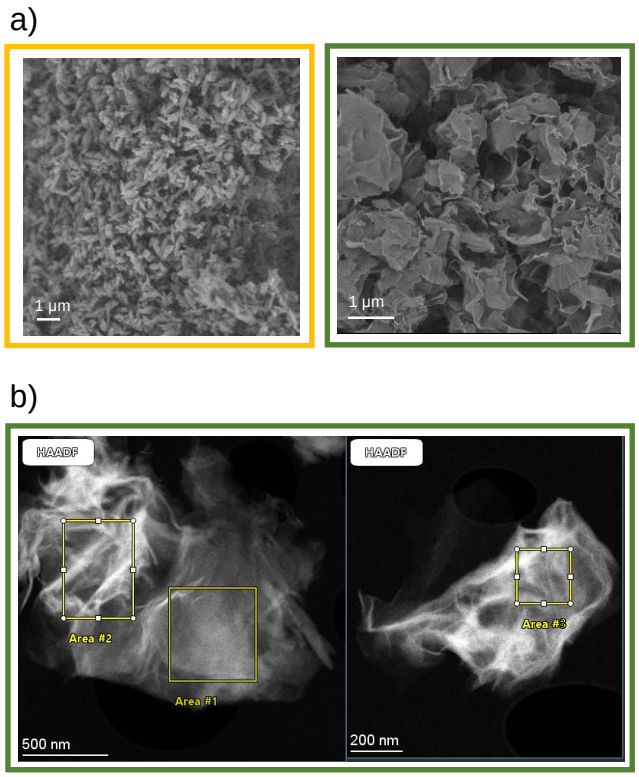

Figure 3. Characterisation of the reaction product between MIL-53(Al)-$(OH)_2$ and 3 eq. of LiOMe in MeOH/THF. a) SEM pictures of the pristine solid (left) and the lithiated solid (right); b) STEM picture of the lithiated product. Areas used for the EDX analyses provided in Table 1 are also shown.

To summarize, all these characterizations eventually indicated that the reaction of MIL-53(Al)-$(OH)_2$ with LiOMe lead to a degradation of the MOF, accompanied with the partial release of Al^{3+}, ultimately leading to a very disordered solid, which presents some structural similarities with Li_4(DOBDC). Furthermore, the use of harsher reactions conditions such as a longer reaction time (15 days) or a higher amount of LiOMe (8 eq. instead of 3) lead eventually to the formation of Li_4(DOBDC), as indicated by PXRD, ICP-AES and STEM-EDX analyses (Figures S6, S17 and S15, respectively). The question then arose whether the final product is simply a mixture of Li_4(DOBDC) with another phase related to MIL-53(Al)-$(OH)_2$, or a new compound. Additional characterisations were carried out to try to answer this question. SEM imaging (Figure 3a) first indicated that the lithiation is accompanied by a strong modification of the morphology of the particles. While the initial MIL-53(Al)-$(OH)_2$ consists of rod-like, crystals shorter than 1 µm, larger (up to few µm) 2-D flake-like particles were finally produced, suggesting that the transformation occurred through a dissolution-reprecipitation mechanism with the formation of a layered structure. This change of morphology was confirmed by TEM

analysis (Figure 3b). As shown in Table 1, EDX analysis carried out on these fluffy particles suggested a rather homogeneous distribution of remaining Al in the solid (note however that few particles of Li_4(DOBDC) were also detected). Analysis of the relative amount of Al, C and O suggested a ligand-to-Al ratio close to 5/2. This result, combined with the ICP analysis, and taking into account the charge balance, gave rise to the tentative formula $Li_7Al(DOBDC)_{5/2}$.

Table 1. Atomic ratios deduced from the STEM-EDX analysis on the area shown in Figure 3. These dara are compared to the ones calculated for $Li_7Al(DOBDC)_{5/2}$.

	Area #1	Area #2	Area #3	average	$Li_7Al(DOBDC)_{5/2}$
C/Al	29	21	20	23	20
C/O	1.4	1.3	1.5	1.4	1.3
O/Al	22	16	12.5	17	15

The solid was eventually studied by X-ray total scattering experiments at the CRISTAL beamline (synchrotron Soleil, France). MIL-53(Al)-$(OH)_2$, the lithiated product and Li_4(DOBDC),

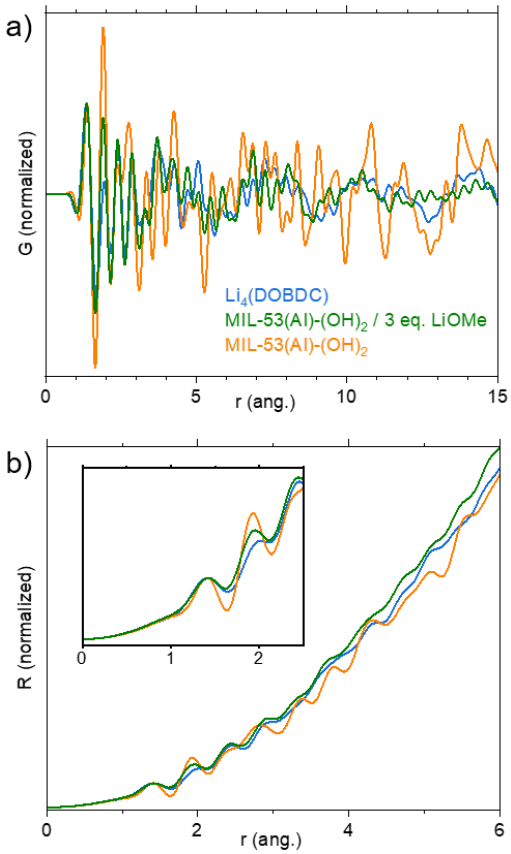

all in a dried form, were compared. The reduced pair distribution function (PDF) G(*r*) and the radial distribution function (RDF) R(*r*) are shown in Figure 4. For both G(*r*) and R(*r*), peaks represent distances between atom pairs. G(*r*) is reduced so that it goes down to 0 when *r* increases; it is particularly suitable to evaluate the order, from low-range to medium-range. When comparing G(*r*) functions of the lithiated solid with MIL-53(Al)-$(OH)_2$ (Figure 4a), the almost complete disappearance of well-defined peaks above 8 Å indicates a lack of order for distances larger than the length of ligand-cation complexes. This is of course in line with the complete amorphization of the solid upon lithiation. R(*r*) takes into account the total number of neighbours, and hence increases in r^2. It is especially adapted to obtain quantitative information at short distances (number of atom pairs). R(*r*) functions were normalized on the peak at 1.4 Å, which corresponds to CC and CO intra-ligand bonds (Figure 4b). The intensity of the peak at 1.9 Å, which is associated with both LiO and AlO bonds, then depends on the atomic number *Z* of the cations bound the oxygen atoms ($I \alpha Z^2$), and to their number *N* ($I \alpha N$). The intensity of this peak decreases in the following order MIL-53(Al)-$(OH)_2$ > lithiated product > Li_4(DOBDC) bonds (Figure 4b, insert). This indicates that less Al-O bonds are present after lithiation (MIL-53(Al)-$(OH)_2$ > lithiated product), but that few of these bonds remain (lithiated product > Li_4(DOBDC)). The fact that the signals of the lithiated product and Li_4(DOBDC) in the range 3-6 Å are not identical is another clear indication that they are truly different compounds. To summarize, the lithiation route based of LiOMe in MeOH/THF leads to the degradation of the pristine MOF, and to the formation of a Li-rich layered phase similar to Li_4(DOBDC), which still contains some aluminium cations. Note that attempts to prepare directly this solid from either $AlCl_3$, LiOMe and H_4DOBDC, or $AlCl_3$ and Li_4(DOBDC), failed (see Figure S13 for the IR spectra), suggesting that the use of the MOF precursor drives, at least to some extent, the formation of $Li_7Al(DOBDC)_{5/2}$.

Figure 4. Characterisation of the reaction product between MIL-53(Al)-$(OH)_2$ and 3 eq. of LiOMe in MeOH/THF by X-ray total scattering experiments. a) Reduced pair distribution function G(*r*); b) radial distribution function R(*r*). Data related to dry MIL-53(Al)-$(OH)_2$, Li_4(DOBDC), and the lithiation product from LiOMe-MeOH/THF, are shown in orange, blue and green, respectively.

The same lithiation strategy was eventually applied to MIL-53(Fe)-$(OH)_2$. As mentioned earlier, this solid presents a low thermal stability, while being highly hydrophilic. The thermogravimetric data (Figure S11) indeed shows that the complete water departure (up to ~155°C) is almost concomitant with the beginning of the degradation of the network (~170°C). Activation under vacuum at 155°C affords a mixture of dehydrated (CP) and hydrated (NP) forms, as indicated by PXRD (Figure S7), but higher temperatures lead to the collapse of the framework. Therefore, the lithiation was carried out on the partially dehydrated solid, using experimental conditions identical to those used for the Al analogue (3 eq. of LiOMe in MeOH/THF at 50°C for 16 hours, and further drying).

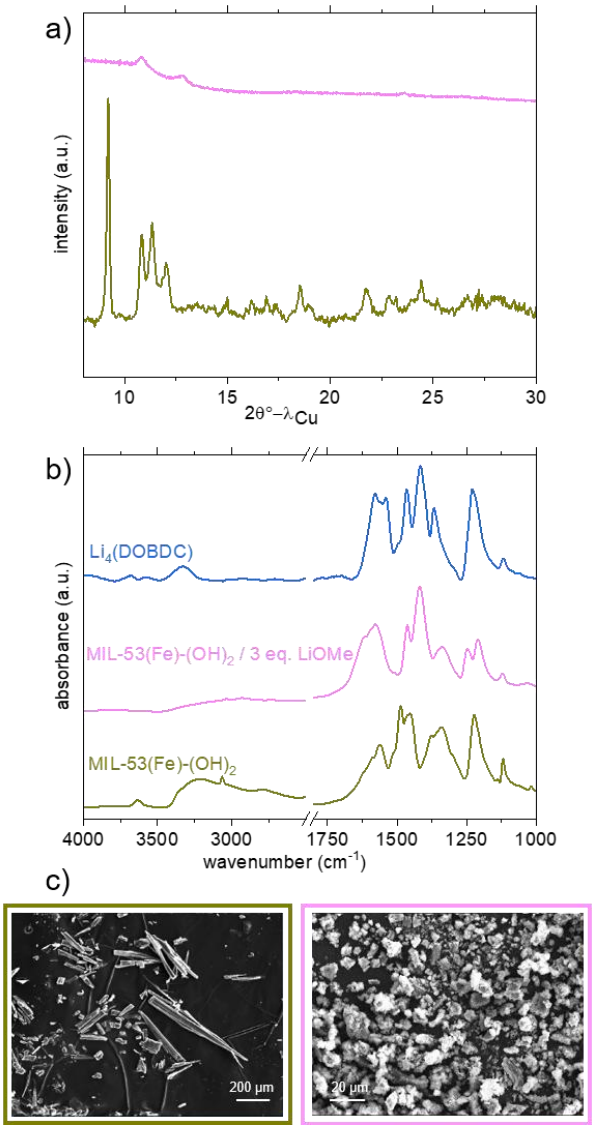

Figure 5. Characterisation of MIL-53(Fe)-$(OH)_2$ and its lithiated product from LiOMe in MeOH/THF. a) PXRD patterns (λ = 1.5406 Å); b) IR spectra; c) SEM pictures. Data related to dry MIL-53(Fe)-$(OH)_2$, Li_4(DOBDC) and the lithiation product are shown in khaki, blue and pink, respectively.

Again, the lithiation reaction is accompanied by a strong change of the PXRD pattern (Figure 5a, pink curve). Two broad peaks at 10.8 and 12.8° are nevertheless still discernible, suggesting that the Fe lithiated product presents some long-range order, contrary to the Al analogue. On the IR spectrum (Figure 5b, pink curve), the band characteristics of the inorganic (3634 cm^{-1}) and organic (3210 cm^{-1}, likely overlapping with the band characteristic of the residual water molecules) OH groups disappear after lithiation, suggesting that the reaction is complete. The vibration bands characteristics of the ligand, notably COO_{asym}, aromatic CC and COO_{sym} at 1618, 1574 and 1461 cm^{-1}, respectively are also shifted, and their position do not match with those found for the salt $Li_4(DOBDC)_4$. Again, no band characteristic of residual solvent molecules was found, in line with the TG curve, which exhibits a clear plateau between 130 and 240°C (Figure S10).
Eventually, the solid was also analysed by ICP analysis after dissolution in a basic aqueous medium (Figure S18). A ratio Li/Fe equal to 3 was measured. This result strongly differs from the one observed for the Al analogue, and suggests that no Fe was released in the reaction

medium, as ultimately confirmed by the analysis of the supernatant. This suggests that the lithiation of MIL-53(Fe)-$(OH)_2$ is successful, and occurs through a pathway different from that observed for MIL-53(Al)-$(OH)_2$. As shown in Figure 5c, SEM analysis showed the initial solid is composed of long (tens to hundreds of µm) needle-like crystals. After lithiation, smaller particles (< 10 µm) are observed, which could result from the breakage of crystals. Contrary to the case of the Al analogue, no evidence of dissolution-reprecipitation steps was detected, in line with the afore-mentioned analyses.

The solid-state electrochemical properties of the lithiated products were then investigated, and compared with those of the pristine MOFs. Composite electrodes prepared by grinding with pestle and mortar the solids with conducting carbon (weight ratio ~2:1) were electrochemically tested in Li half-cells under galvanostatic cycling conditions at one electron exchanged per ligand in 15 hours, the electrolyte consisting first in 1 M $LiClO_4$ in propylene carbonate. Considering the previous reports on DOBDC derived materials and MIL-53(Fe), experiments were carried out starting in oxidation, within the potential window $2.2 \leq E \leq 3.8$ V *vs.* Li^+/Li.

The first and fifth cycles are shown Figure 6. For pristine MIL-53(Al)-$(OH)_2$, no significant activity was detected, as expected (see the orange curve on Figure 6a). For the derived product obtained upon reaction with LiH in DMF (Figure 6a, red curve), a short plateau centered at 3.45 V is detected during the first oxidation. This redox potential could match with the one of DOBDC when interacting with a cation of high ionic potential (here Al^{3+}).[12] Nevertheless, the capacity is moderate, and found to be mostly irreversible from the first reduction and upon further cycling obliterating the practical interest of such a solid.

The behavior of the product lithiated with LiOMe is different (Figure 6a, green curve). The potential at rest (open circuit voltage, OCV) is lower (~2.6 instead of ~3 V *vs.* Li^+/Li for other solids), in line with the instability of this solid in air (see above). During the first oxidation, a gradual oxidation is observed up to 3.8 V, and associated with a high capacity (> 200 mAh g^{-1}). Nevertheless, more than half of this capacity is lost during the first reduction, and further decreased during the following cycles. As mentioned earlier, the question arose whether this compound is related to the salt Li_4(DOBDC). The cycling behavior of Li_4(DOBDC) and this solid are compared in Figure 7a on a narrower potential range (2.2-3.2 V *vs.* Li^+/Li). It is clearly seen that the average redox potential of the lithiated MIL-53(Al)-$(OH)_2$ is significantly higher (+180 mV) that the one of Li_4(DOBDC) (2.76 vs 2.58 V *vs.* Li^+/Li, respectively). As initially demonstrated for $MgLi_2$(DOBDC), the presence of a cation with a high ionic potential close to the DOBDC redox unit dramatically increases the oxidation potential of phenolate moieties.[12] This suggests that Al^{3+} cations remain close to the ligand, in line with other characterizations.

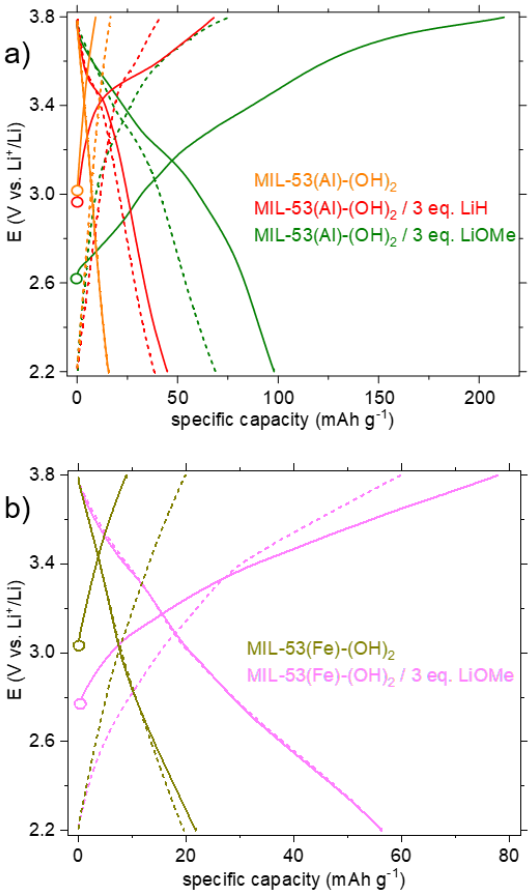

Figure 6. Electrochemical behaviour upon galvanostatic cycling in Li half-cells of the lithiated products compared to the pristine MOFs materials (electrolyte: 1 M $LiClO_4$ in PC): potential vs. specific capacity curves. Plain lines correspond to the 1st cycle, dashed lines to the 5th cycle. a) Data related to dry MIL-53(Al)-$(OH)_2$, and lithiation products from LiH-DMF and LiOMe-MeOH/THF, are shown in orange, red and green, respectively; b) data related to the lithiation product of MIL-53(Fe)-$(OH)_2$ from LiOMe-MeOH/THF.

Finally, the cyclability of this solid was evaluated within this potential range. As shown in Figure 7b, the reversible capacity reached ca. 40 mAh g^{-1}, with a rather good capacity retention (-12% after 15 cycles). Considering this initial result, a very-long term evaluation of the capacity retention was further carried out, that time using a solid obtained treated with 4 eq. of LiOMe instead of 3. Both solids present the same composition $Li_7Al(DOBDC)_{5/2}$, as proven by IR, STEM-EDX and ICP-AES analyses (see Figures S14, S16 and S17, respectively). As shown in Figure 8a, using identical cycling conditions (potential range and cycling rate), the capacity remained almost constant for more than 900 cycles corresponding to more than one year in operation. Such an outstanding capacity retention paired with a perfectly stable electrochemical feature upon cycling demonstrate that the small amount of Al^{3+} bounded to the redox-active ligands is amazingly stable (Figure 8b). Note that this lithiated product does not evolve towards $Li_4(DOBDC)$ probably due to the trivalent state of Al^{3+} that does not favor any ion exchange reaction with Li^+ ions contained in the electrolyte.

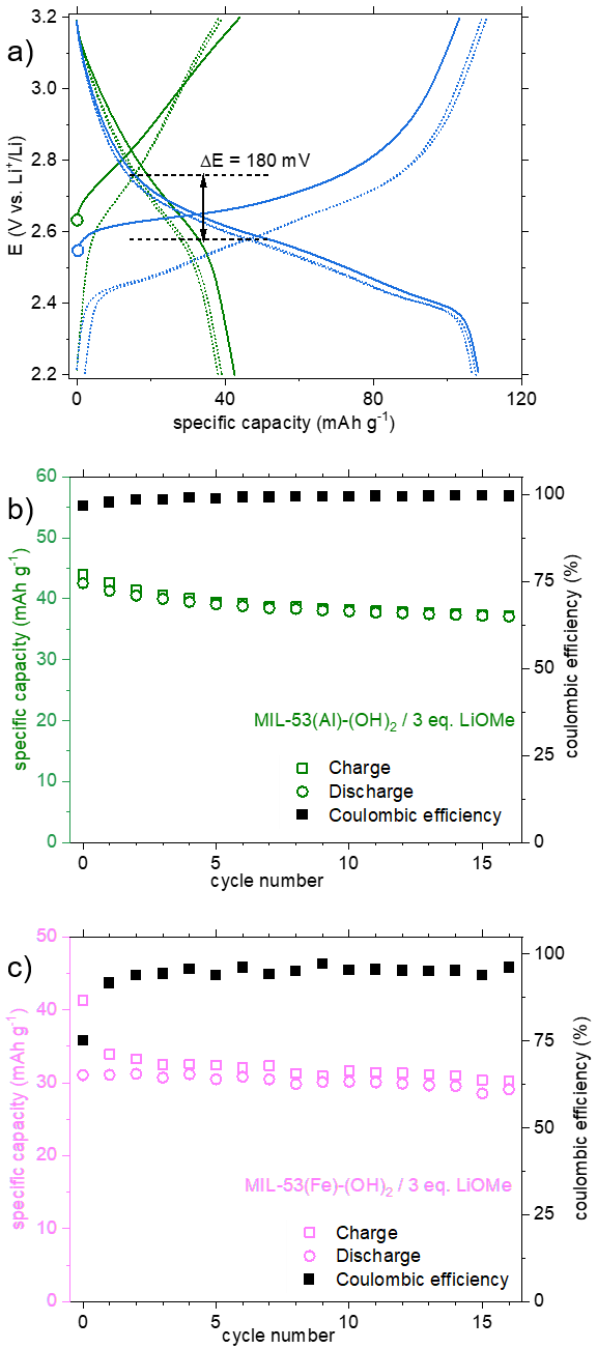

Figure 7. a) Comparison of potential *vs.* specific capacity curves for Li_4(DOBDC) (blue) and the lithiation product from MIL-53(Al)-$(OH)_2$ and LiOMe-MeOH/THF (green). Plain lines correspond to the 1st cycle, dashed lines to the 5th and 10th cycles; b) capacity retention and coulombic efficiency for the lithiation product from MIL-53(Al)-$(OH)_2$ and LiOMe-MeOH/) (electrolyte: 1 M $LiClO_4$ in PC; potential range: 2.2-3.2 V vs. Li^+/Li); c) capacity retention and coulombic efficiency for the lithiation product from MIL-53(Fe)-$(OH)_2$ and LiOMe-MeOH/) (electrolyte: 1 M $LiPF_6$ in 1:1 EC:DMC; potential range: 2.2-3.6 V vs. Li^+/Li).

Eventually, an electrochemical study was also conducted on the lithiated product obtained from the reaction of MIL-53(Fe)-$(OH)_2$ with LiOMe. Again, compared to the pristine MOF, a significant activity was detected during the first oxidation of the lithiated derivative (Figure

6b, pink curve), with a continuous increase of the capacity up to ~ 80 mAh g^{-1} at 3.8 V, likely associated with the oxidation of the ligand. The capacity is slightly lower during the first reduction (57 mAh g^{-1}). Knowing that the reduction of Fe^{3+} to Fe^{2+} occurs at ~3.0 V in the parent MIL-53(Fe)[8] and in the pristine MIL-53(Fe)-$(OH)_2$ (Figure 6b, khaki curve), the absence of additional capacity upon reduction suggests that the Fe^{3+} ions are inactive in our experimental conditions. This might relate to the fact that the solid already contain 3 Li^+ per iron, and cannot accommodate the additional Li^+ that would be necessary to balance the charge of Fe^{2+}. The capacity retention of this solid was nevertheless evaluated in the potential range 2.2-3.6 V *vs.* Li^+/Li (Figure 7c). From the second cycle, the capacity appears rather constant (-6% after 15 cycles), but reaches only ~30 mAh g^{-1}, corresponding to the reversible insertion of only ~0.3 electron per $Li_3FeO(DOBDC)$.

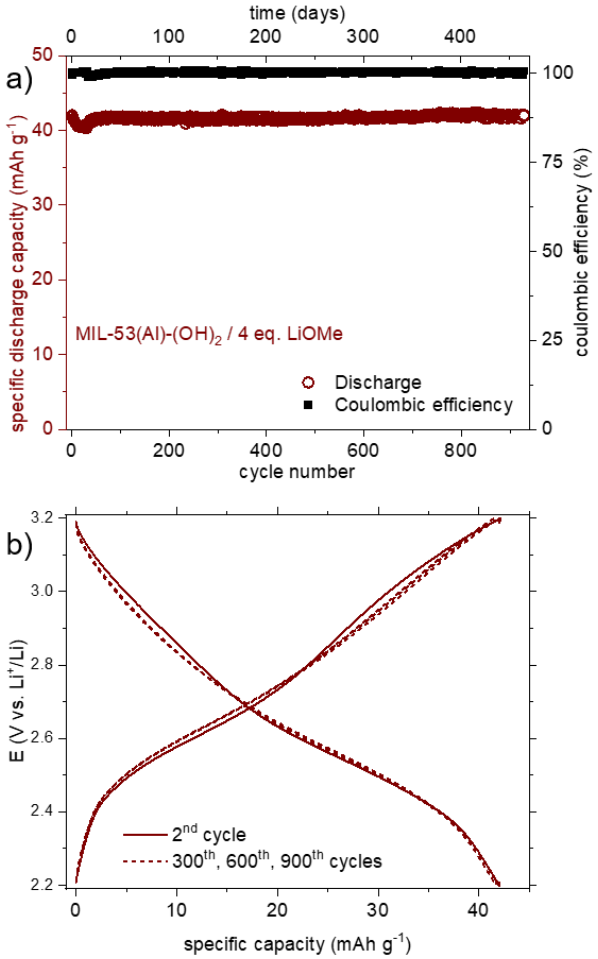

Figure 8. a) Potential *vs.* specific capacity curves for the lithiation product from MIL-53(Al)-$(OH)_2$ and LiOMe-MeOH/THF. Plain lines correspond to the 2nd cycle, dashed lines to the 300th, 600th and 900th cycles; b) capacity retention and coulombic efficiency for the lithiation product from MIL-53(Al)-$(OH)_2$ and 4 eq. of LiOMe (electrolyte: 1 M $LiClO_4$ in PC; potential range: 2.2-3.2 V vs. Li^+/Li).

Conclusions

The reactivity of functionalised MIL-53(M)-$(OH)_2$ (M= Al, Fe) with various strong bases was studied, with the aim at fully exchanging the acidic protons (both organic and inorganic) by Li^+ ions to ultimately exploit the redox activity of the phenolic ligand in the solid state. This reactivity was found to strongly depend on the nature of the base (LiH *vs.* LiOMe) and of the

cation. More specifically, whereas it was not possible to fully deprotonate MIL-53(Al)-$(OH)_2$ with LiH in DMF, the reaction with LiOMe in MeOH/THF lead to a partial release of Al^{3+} and the formation of an amorphous layered phase formulated $Li_7Al(DOBDC)_{5/2}$. In contrast, the lithiation of the Fe analogue occurred without leaching, leading to the expected composition $Li_3FeO(DOBDC)$. In both cases, the electrochemical activity of the ligand in the solid state was detected. The associated reversible capacities are moderate, but a shift of the redox potential compared to those of the salt $Li_4(DOBDC)$ is observed, together with an outstanding capacity retention (> 900 cycles, > one year), at least for one solid. Although these lithiated MOF derivatives are of limited practical interest for electrochemical energy storage, this study eventually suggests that it is possible to expand the scope of polycations (from +2+ to +3) suitable to tune the redox potential of the ligand, and to use them in small amounts (as "dopants") in the layered $Li_4(DOBDC)$-type structure.

Author Contributions

MD: synthesis, XRD and IR characterization and electrochemical evaluation; HC: PDF analysis; PM: STEM-EDX analysis; ND and MP: NMR analysis; PP: conceptualization and electrochemical analysis; TD: conceptualization, spectroscopic analysis and writing.

Conflicts of interest

There are no conflicts to declare.

Acknowledgements

Fundings from the region Pays de la Loire (project PSR 'MatHySE2') and the Agence Nationale de la Recherche (project 'ThiOMOFs') is acknowledged (fellowships for M.D. and P.S-A., respectively). Funding by the French Contrat Plan État-Région and the European Regional Development Fund of Pays de la Loire, the CIMEN Electron Micros-copy Center in Nantes, is gratefully acknowledged. P. Deniard is thanked for his advice for the PDF analysis, and S. Grolleau for the thermal analyses. A. Vlad (UCLouvain) is acknowledged for fruitful discussions. The authors also thank the synchrotron Soleil for providing access to the beamline Cristal Soleil. The ICP-AES analyses were performed at the LPG-UMR 6112 (C. La, M. Rivoal), Nantes Université.

Notes and references

1 J. Zhou and B. Wang, *Chem. Soc. Rev.*, 2017, **46**, 6927–6945.
2 Y. Xu, Q. Li, H. Xue and H. Pang, *Coord. Chem. Rev.*, 2018, **376**, 292–318.
3 L. Zhang, H. Liu, W. Shi and P. Cheng, *Coord. Chem. Rev.*, 2019, **388**, 293–309.
4 Z. Wang, H. Tao and Y. Yue, *ChemElectroChem*, 2019, **6**, 5358–5374.
5 J. Liu, D. Xie, W. Shi and P. Cheng, *Chem. Soc. Rev.*, 2020, **49**, 1624–1642.
6 A. Schneemann, R. Dong, F. Schwotzer, H. Zhong, I. Senkovska, X. Feng and S. Kaskel, *Chem. Sci.*, 2021, **12**, 1600–1619.
7 T. Devic, in *Metal-Organic Frameworks in Biomedical and Environmental Field*, Springer Nature, P. Horcajada and S. Rojas., 2021, pp. 111–154.
8 G. Férey, F. Millange, M. Morcrette, C. Serre, M.-L. Doublet, J.-M. Grenèche and J.-M. Tarascon, *Angew. Chem. Int. Ed.*, 2007, **46**, 3259–3263.
9 C. Costentin, M. Robert and J.-M. Savéant, *J. Am. Chem. Soc.*, 2006, **128**, 8726–8727.
10 S. Renault, S. Gottis, A.-L. Barres, M. Courty, O. Chauvet, F. Dolhem and P. Poizot, *Energy Environ. Sci.*, 2013, **6**, 2124–2133.
11 S. Wang, L. Wang, K. Zhang, Z. Zhu, Z. Tao and J. Chen, *Nano Letters*, 2013, **13**, 4404–4409.

12 A. Jouhara, N. Dupré, A.-C. Gaillot, D. Guyomard, F. Dolhem and P. Poizot, *Nature Commun.*, 2018, **9**, 4401.
13 P. D. C. Dietzel, Y. Morita, R. Blom and H. Fjellvåg, *Angew. Chem. Int. Ed.*, 2005, **44**, 6354–6358.
14 N. L. Rosi, J. Kim, M. Eddaoudi, B. Chen, M. O'Keeffe and O. M. Yaghi, *J. Am. Chem. Soc.*, 2005, **127**, 1504–1518.
15 M. Maercz, D. S. Wragg, P. D. C. Dietzel and H. Fjellvag, *Acta Cryst.*, 2013, **E69**, m152.
16 F. Luo, C. Yan, L. Dang, R. Krishna, W. Zhou, H. Wu, X. Dong, Y. Han, T.-L. Hu, M. O'Keeffe, L. Wang, M. Luo, R.-B. Lin and B. Chen, *J. Am. Chem. Soc.*, 2016, **138**, 5678–5684.
17 H. Assi, L. C. Pardo Pérez, G. Mouchaham, F. Ragon, M. Nasalevich, N. Guillou, C. Martineau, H. Chevreau, F. Kapteijn, J. Gascon, P. Fertey, E. Elkaim, C. Serre and T. Devic, *Inorg. Chem.*, 2016, **55**, 7192–7199.
18 H. Chun and D. Moon, *Crystal Growth Des.*, 2017, **17**, 2140–2146.
19 P. C. Dietzel, R. Blom and H. Fjellvåg, *Z. Anorg. Allg. Chem.*, 2009, **635**, 1953–1958.
20 T. Devic, P. Horcajada, C. Serre, F. Salles, G. Maurin, B. Moulin, D. Heurtaux, G. Clet, A. Vimont, J.-M. Grenèche, B. L. Ouay, F. Moreau, E. Magnier, Y. Filinchuk, J. Marrot, J.-C. Lavalley, M. Daturi and G. Férey, *J. Am. Chem. Soc.*, 2010, **132**, 1127–1136.
21 P. Horcajada, F. Salles, S. Wuttke, T. Devic, D. Heurtaux, G. Maurin, A. Vimont, M. Daturi, O. David, E. Magnier, N. Stock, Y. Filinchuk, D. Popov, C. Riekel, G. Férey and C. Serre, *J. Am. Chem. Soc.*, 2011, **133**, 17839–17847.
22 D. Cunha, C. Gaudin, I. Colinet, P. Horcajada, G. Maurin and C. Serre, *J. Mater. Chem. B*, 2013, **1**, 1101–1108.
23 M. L. Aubrey and J. R. Long, *J. Am. Chem. Soc.*, 2015, **137**, 13594–13602.
24 D. Rambabu, A. E. Lakraychi, J. Wang, L. Sieuw, D. Gupta, P. Apostol, G. Chanteux, T. Goossens, K. Robeyns and A. Vlad, *J. Am. Chem. Soc.*, 2021, **143**, 11641–11650.
25 S. Biswas, T. Ahnfeldt and N. Stock, *Inorg. Chem.*, 2011, **50**, 9518–9526.
26 J. Rodriguez-Carvajal, *Physica B*, 1993, **192**, 55.
27 D. Massiot, F. Fayon, M. Capron, I. King, S. Le Calvé, B. Alonso, J. O. Durand, B. Bujoli, Z. Gan and G. Hoatson, *Magn. Reson. Chem.*, 2002, **40**, 70.
28 P. Juhás, T. Davis, C. L. Farrow and S. J. L. Billinge, *J. Appl. Cryst.*, 2013, **46**, 560–566.
29 K. L. Mulfort and J. T. Hupp, *J. Am. Chem. Soc.*, 2007, **129**, 9604–9605.
30 K. L. Mulfort and J. T. Hupp, *Inorg. Chem.*, 2008, **47**, 7936–7938.
31 K. L. Mulfort, T. M. Wilson, M. R. Wasielewski and J. T. Hupp, *Langmuir*, 2009, **25**, 503–508.
32 N. Biggins, M. E. Ziebel, M. I. Gonzalez and J. R. Long, *Chem. Sci.*, 2020, **11**, 9173–9180.
33 K. L. Mulfort, O. K. Farha, C. L. Stern, A. A. Sarjeant and J. T. Hupp, *J. Am. Chem. Soc.*, 2009, **131**, 3866–3868.
34 Dieter Himsl, Dirk Wallacher and Martin Hartmann, *Angew. Chem. Int. Ed.*, 2009, **48**, 4639–4642.
35 K. Riascos-Rodríguez, S. Marks, P. G. Evans, S. P. Hernández-Rivera, J. L. Ruiz-Caballero, D. Piñero and A. J. Hernández-Maldonado, *Crystal Growth Des.*, 2020, **20**, 3898–3912.
36 M. Kubo, H. Hagi, A. Shimojima and T. Okubo, *Chem. Asian J.*, 2013, **8**, 2801–2806.
37 Y.-S. Bae, B. G. Hauser, O. K. Farha, J. T. Hupp and R. Q. Snurr, *Microporous Mesoporous Mater.*, 2011, **141**, 231–235.
38 F. Millange and R. I. Walton, *Israel J. Chem.*, 2018, **58**, 1019–1035.
39 Z. Wang, A. Bilegsaikhan, R. T. Jerozal, T. A. Pitt and P. J. Milner, *ACS Appl. Mater. Interfaces*, 2021, **13**, 17517–17531.
40 S. Renault, J. Geng, F. Dolhem and P. Poizot, *Chem. Commun.*, 2011, **47**, 2414–2416.
41 T. Loiseau, C. Serre, C. Huguenard, G. Fink, F. Taulelle, M. Henry, T. Bataille and G. Férey, *Chem. Eur. J.*, 2004, **10**, 1373–1382.